

Conformational Polymorphism of the PrP106–126 Peptide in Different Environments: A Molecular Dynamics Study

Alessandra Villa,^{*,†} Alan E. Mark,[†] Gloria A. A. Saracino,[‡] Ugo Cosentino,[‡] Demetrio Pitea,[‡] Giorgio Moro,^{*,§} and Mario Salmona^{||}

Groningen Biomolecular Sciences and Biotechnology Institute (GBB), University of Groningen, Nijenborgh 4, 9747 AG Groningen, The Netherlands, Dipartimento di Scienze dell'Ambiente e del Territorio, University of Milano-Bicocca, P.zza dell'Ateneo Nuovo 1, 20126 Milano, Italy, Dipartimento di Biotecnologie e Bioscienze, University of Milano-Bicocca, P.zza dell'Ateneo Nuovo 3, 20126 Milano, Italy, and Istituto Mario Negri, Via Eritrea 62, 20157 Milano, Italy

Received: May 24, 2005; In Final Form: November 4, 2005

Extensive molecular dynamic simulations (~240 ns) have been used to investigate the conformational behavior of PrP106–126 prion peptide in four different environments (water, dimethyl sulfoxide, hexane, and trifluoroethanol) and under both neutral and acidic conditions. The conformational polymorphism of PrP106–126 in solution observed in the simulations supports the role of this fragment in the structural transition of the native to the abnormal form of prion protein in response to changes in the local environmental conditions. The peptide in solution is primarily unstructured. The simulations show an increased presence of helical structure in an apolar solvent, in agreement with the results from circular dichroism spectroscopy. In water solution, β -sheet elements were observed between residues 108–112 and either residues 115–121 or 121–126. An α – β transition was observed under neutral conditions. In DMSO, the peptide adopted an extended conformation, in agreement with nuclear magnetic resonance experiments.

Introduction

Prion diseases^{1,2} are transmissible neurodegenerative disorders characterized by the accumulation of abnormal forms of prion protein (PrP^{Sc}) in nervous tissue.^{3,4} In contrast with the native form of the protein (PrP^C), PrP^{Sc} is partly resistant to protease digestion, binds nonspecifically to membranes, and forms insoluble amyloidogenic fibrils.³ The accumulation of these amyloid aggregates in the brain is correlated with the degeneration of nerve cells. Transformation of the PrP^C into the self-propagating PrP^{Sc} form involves a conformational change associated with a decrease in α -helical secondary structure and a marked increase in β -sheet content.⁴ Structural studies⁵ show that the normal protein is composed of two structurally distinct moieties: an extended N-terminus segment (residues 23–125) with features of a flexible disordered peptide chain, and a well-defined globular domain (residues 126–231) with three α -helices and a two-stranded antiparallel β -sheet. The structure of the infectious form PrP^{Sc}, in contrast, is not known in detail due to its complex, noncrystalline polymeric nature.

Experimental studies have shown that a synthetic homologue of residues 106–126 of human PrP (PrP106–126) exhibits some properties typical of PrP^{Sc}. These include neurotoxicity, an ability to activate astroglial and microglial cells,⁶ and a tendency to aggregate into amyloid fibrils that are partly resistant to protease digestion.⁷ Moreover, PrP106–126 shows remarkable

polymorphism, acquiring different secondary structures in different environments, as evidenced by circular dichroism (CD) spectroscopy^{8,9} and nuclear magnetic resonance (NMR) experiments.^{10,11} These have shown that the chemical-physical conditions, such as pH, ionic strength, and solvent composition all influence the secondary structure of the peptide. Because of these properties, the PrP106–126 peptide is a widely studied model system for the *in vitro* investigation of the pathological PrP protein. The PrP106–126 peptide consists of an N-terminal polar head (Lys-Thr-Asn-Met-Lys-His-Met), followed by a long hydrophobic tail (Ala-Gly-Ala-Ala-Ala-Ala-Gly-Ala-Val-Val-Gly-Gly-Leu-Gly).

The conformational transition from PrP^C to PrP^{Sc} appears modulated by the nature of the surrounding medium. However, the different experimental and theoretical studies that have been conducted to date have failed to yield a consistent picture of the underlying mechanism. Nevertheless, the strategic position of segment 106–126 lying between the structured and unstructured domains of the prion protein means that this region is a prime candidate to play a key role in the structural transition of PrP^C to PrP^{Sc}.

In this work, molecular dynamics (MD) simulations are used to study the effect of the surrounding medium on the structural properties of PrP106–126. The complete characterization of this peptide in isolation has proved difficult to achieve by using experimental techniques such as X-ray crystallography and liquid-state NMR. This is due to the tendency of PrP106–126 to form fibrils that have a complex, noncrystalline polymeric structure. Computational approaches, however, allow us to obtain a description of the peptide at a microscopic level. Here, we present an investigation of the peptide as an “isolated” molecule in solution. In addition, the charges on the termini of PrP106–126 have been removed, while the majority of experimental studies on PrP106–126 have been carried out on the

* Corresponding authors. villa@theochem.uni-frankfurt.de (A.V.); giorgio.moro@unimib.it (G.M.). Current address (A.V.): Institute for Physical and Theoretical Chemistry, J. W. Goethe University, Marie Curie Strasse 11, 60439 Frankfurt am Main, Germany.

[†] Groningen Biomolecular Sciences and Biotechnology Institute (GBB).

[‡] Dipartimento di Scienze dell'Ambiente e del Territorio, University of Milano-Bicocca.

[§] Dipartimento di Biotecnologie e Bioscienze, University of Milano-Bicocca.

^{||} Istituto Mario Negri.

uncapped peptide. We have made such a choice mainly for two main reasons. First, the AcPrP106–126 NH₂ peptide mimics better the sequence inserted in protein than the unblocked one. Second, experimentally, it has been observed that the removal of the C-terminus charge of amyloid peptides by amidation inhibits fibril formation.^{9,12}

PrP106–126 peptide^{11,13} and the slightly different PrP portion, PrP109–122,¹⁴ have been the subject of several previous theoretical studies. Levy et al.¹³ carried out four 1–2 ns explicit solvent MD simulations and 30 implicit solvent MD simulations to study the helix–coil transition of PrP106–126 in water solutions. They concluded that the α -helix conformation at neutral condition is rather unstable, and they suggested that the helix–coil transition is governed by hydrophobic interaction between His111 and Val122. Furthermore, Kuwata et al.¹¹ used MD techniques to gain insight into the possible structural properties of fibrils. In this work, MD is used to study the conformational polymorphism of the peptide in different environments. The peptide was simulated in four solvents of different polarity. The effect of varying the pH was mimicked by changing the protonation state of amino acid side chains. The results were compared with experimental data, taking into account the fact that the simulation conditions correspond to a highly dilute solution (no aggregation).

Computational Technique

The simulations were performed of the C-terminal amidated and the N-terminal acetylated forms of PrP106–126. Two starting conformations were used: an ideal α -helix and a β -hairpin modeled on the basis of the X-ray study of Inouye and Kirschner.¹⁵ One simulation was also started from a completely extended configuration. All the model structures were built by using the software MAESTRO.¹⁶ The peptide was described by using the GROMOS96 (43a2) force field,¹⁷ in which aliphatic hydrogen atoms are treated as united atoms, together with the carbon atom to which they are attached. The charges of ionizable groups were chosen appropriate for pH 7.0: the lysines were protonated and the histidine was singularly protonated and the N ϵ 2–H tautomer was chosen. This form of the peptide has been labeled HIS. To mimic PrP106–126 under acidic conditions, the double protonated form of the histidine was used (simulation HISH). Note that, as it is not possible to have partial protonation states, it was assumed that histidine is singularly protonated at pH 7, even though the pK_a of histidine is around 6.0.

The peptide was solvated in four different solvents: water, dimethyl sulfoxide (DMSO), hexane, and trifluoroethanol (TFE). Explicit solvent models were used. Specifically, the SPC model for water was used.¹⁸ For the other solvents, models developed to be compatible with the GROMOS force field (DMSO,¹⁹ hexane,¹⁷ and TFE²⁰) were used. No counterions were added. The total charge of the system was +1 for the HIS form of the peptide and +2 for the HISH form. The question of whether counterions should be added to balance the overall charge in simulations is a matter of continuing debate. In this regard, it should be noted that, because of the small-sized box, adding ions to balance the charge in this system would lead to very high effective salt concentration, which could affect the stability of the system. Thus, in order that a direct comparison with the experimental data could be made, no counterions were added. This also avoided difficulty associated with the very slow equilibration of the ion distribution.

All simulations were performed by using the GROMACS (version 3.0) package²¹ in a periodic triclinic box. Two box

TABLE 1: Details of the Simulations Performed^a

starting structure	His111	solvent	simulation time
α -helix	HIS	water	60 ns, 10 ns ^b , 10 ns ^b , 10 ns, 10 ns
	HISH	water	60 ns, 10 ns, 10 ns, 10 ns, 10 ns
	HIS	DMSO	60 ns, 10 ns, 10 ns, 10 ns, 10 ns
	HIS	hexane	60 ns, 10 ns, 10 ns, 10 ns, 10 ns
	HIS	TFE	60 ns, 10 ns, 10 ns, 10 ns, 10 ns
β -hairpin	HIS	water	40 ns, 40 ns, 30 ns, 10 ns, 20 ns
	HISH	water	40 ns, 40 ns, 30 ns, 10 ns, 20 ns
	HIS	DMSO	40 ns, 40 ns, 10 ns, 10 ns, 40 ns
	HIS	hexane	40 ns, 40 ns, 10 ns, 10 ns, 40 ns
	HIS	TFE	40 ns, 40 ns, 10 ns, 10 ns, 40 ns
extended	HIS	water	10 ns

^a Italicized values correspond to the simulations performed in the largest box. ^b Simulations extended to 60 ns during the work.

volumes were used: 154 and 364 nm³, respectively. They were filled with around 4900 and 11 900 water molecules, 1100 and 2800 DMSO molecules, 600 and 1400 hexane molecules, and 1100 and 2800 TFE molecules, respectively. The distance between the peptide atoms and their periodic images was always greater than 1.5 nm. The simulation started from the extended conformation was performed in a box of 21 000 water molecules (649 nm³).

Nonbonded interactions were evaluated by using a twin-range cutoff: interactions within the shorter-range cutoff (0.9 nm) were evaluated every step, whereas interactions within the longer cutoff (1.4 nm) were updated every 5 steps, together with the pair list. To correct for the neglect of electrostatic interactions beyond the 1.4 nm cutoff, a reaction field (RF) correction²² was used. The ϵ_{RF} values used are 78.0 for water, 47.0 DMSO, 6.0 for hexane, and 26.7 for TFE. To maintain constant temperature and pressure, a Berendsen thermostat²³ was applied. The peptide and the solvent were independently coupled to a temperature bath ($T = 298$ K), with a coupling time of 0.1 ps. The pressure²³ was held at 1 bar, with a coupling time of 0.5 ps for water, 1.0 ps for DMSO, 2.0 ps for hexane, and 4.0 ps for TFE. The isothermal compressibility was set to $4.6 \cdot 10^{-5}$ bar⁻¹ for water, $5.2 \cdot 10^{-5}$ bar⁻¹ for DMSO, $11.2 \cdot 10^{-5}$ bar⁻¹ for hexane, and $12.2 \cdot 10^{-5}$ bar⁻¹ for TFE. The time step was 0.002 ps. The bond lengths and angle in water were constrained by using the SETTLE algorithm.²⁴ Bond lengths within the peptide and other solvents were constrained by using the LINCS algorithm.²⁵ The initial velocities of the atoms were taken from a Maxwell distribution at 298 K. Different random number seeds were used for each simulation. The systems were simulated for a minimum of 10 ns to a maximum of 60 ns. Before carrying out the MD simulations, a steepest descent minimization was performed. In Table 1, the details of the simulations performed are reported.

The solvent accessible surface (SAS) was computed numerically.²⁶ The atomic radii used were 0.16 nm for carbon, 0.13 nm for oxygen, 0.14 nm for nitrogen, 0.20 nm for sulfur, and 0.10 nm for hydrogen atoms. The atomic radius of the solvent was 0.14 nm. An atom was defined as hydrophilic when the module of its partial charge was equal to or bigger than 0.2 e⁻. The secondary structure element analysis was based on the definitions of Kabsch–Sander.²⁷ To define the presence of an H-bond, an acceptor–hydrogen distance within 0.25 nm and acceptor–hydrogen–donor angle within 60° was used.

The proton–proton vicinal coupling constants between the amide proton and the C $^{\alpha}$ -proton ($^3J_{H_N,H_{\alpha}}$) were estimated from the simulations by using the Karplus relation:²⁸

$$^3J_{H_N,H_{\alpha}} = A \cos^2 \theta + B \cos \theta + C \quad (1)$$

where θ is the dihedral angle between the planes determined

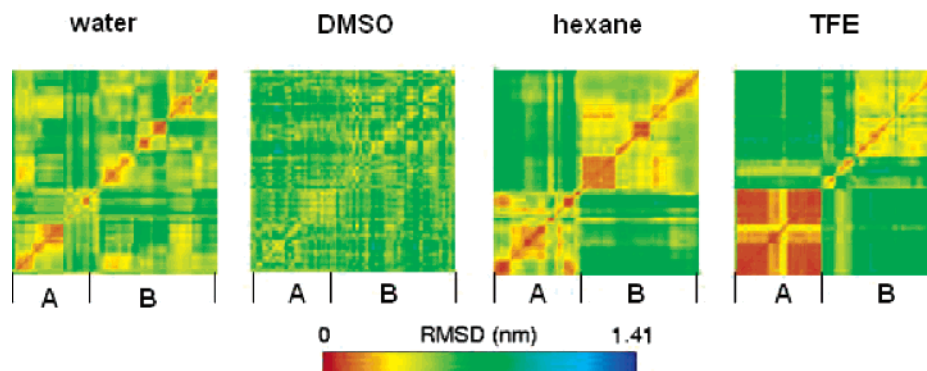


Figure 1. RMSD matrix for each structure from the HIS simulations of PrP106–126 (see Table 1) with respect to all other structures generated in the same environment. RMSD values (nm) for the backbone atoms of residue 107–125 evaluated after performing a least-squares best fit on the same atoms.

by $H-C^{\alpha}-N$ and $C^{\alpha}-N-H$, respectively. The values used for the empirical constants A, B, and C are 6.51, -1.76 , and 1.6, respectively.²⁹

Results and Discussion

The PrP106–126 peptide was simulated in four solvents: water, DMSO, hexane, and TFE. In aqueous solution, two forms of peptide were considered: HIS, where His111 is mono-protonated to mimic pH 7, and HISH form, where His111 is fully protonated to mimic acidic conditions. For each peptide–solvent system, 10 independent simulations were performed (Table 1). These differed in the starting configuration (α -helix or β -hairpin), the initial velocities, and the box dimensions. A total of 240 ns of simulation was performed for each system. The simulations are labeled A when the starting structure is an α -helix, and B when it is a β -hairpin.

The simulations suggest that the behavior of the peptide depends significantly on the solvent environment. Figure 1 shows matrixes of the root-mean-square deviation (RMSD) values for the backbone atoms of each structure with respect to all other structures generated in the same environment. The presence of light-colored, off-diagonal regions indicates the sampling of similar regions of conformational space. Despite the difference in the starting structures, the simulations in water solutions started either from an α -helix or a β -hairpin show overlapping regions (Figure 1). In DMSO, the initial structure is lost rapidly, and it is not possible to distinguish the regions of the matrix belonging to different simulations. In the case of the hexane and TFE simulations, the appearance of the RMSD matrix is quite different. The color distribution is inhomogeneous. For both of the systems, two regions along the diagonal, one corresponding to the A set and the other to the B set, are evident. In none of the systems investigated was it possible to see specific effects of changing the starting velocities and/or the dimensions of the box on the sampling of the conformational space.

The effect of the media is also reflected in the exposure of the peptide to the solvent. The average exposure of the hydrophobic groups to solvent in water (11.4 nm^2) is less than that in DMSO (15.3 nm^2) or hexane (12.6 nm^2). Hydrophilic groups are less exposed to solvent in hexane. The final values for the solvent-accessible surface were independent of the starting structure in all simulations except those in TFE.

To understand the effect of the environment on the conformational behavior of PrP106–126, the presence of elements of secondary structure as a function of time was analyzed. In general, α -helical elements appeared only in simulations started from an α -helix. Elements of a β -sheet appeared more frequently

in simulations initiated from a β -hairpin, but in water solution, a β -sheet was also observed in simulations starting from an α -helix. Figure 2 shows the secondary structure as a function of time for some of the simulations in aqueous solution, together with representative configurations. When His111 is singularly protonated in water (mimicking neutral pH), the tendency to form a β -sheet is higher than in the simulations that mimic acidic conditions. At neutral pH, an α -helix to β -sheet transition occurred after 2 ns (Figure 2). To examine the probability of an α – β transition occurring, two other simulations started from an α -helix were extended to 60 ns. In both the simulations, a roughly stable conformation was observed during the last 30 ns: one resembled a hairpin and the other contained persistent elements of α -helix (structure 3Aw in Figure 2). Elements of a β -sheet were also observed in the B set after 2 ns (see structure 1Bw in Figure 2) and in the 10 ns simulation started from a completely extended conformation. The β -sheet elements observed in water involved either the residues 108–112 and 115–121 (such as structures 1Aw and 1Bw in Figure 2) or the residues 108–112 and 121–126 (such as structure 2Aw). When the His111 is double protonated (mimicking acid pH), the hydrophilic core of the peptide shows a persistent α -helix conformation in the A set (initial structure α -helical), while the predominant conformations of the B set resembled a hairpin. In general, the results agree with those obtained by Levy et al.¹³ and support the hypothesis that, at neutral pH, the helix–coil transition is governed by the hydrophobic interaction involving His111, while at acidic pH, the effect of these stabilizing interaction is reduced because of the protonation of the histidine.

Table 2 shows the percentage of helix, β -sheet, and random coil for each system observed in the MD simulations. Experimentally, data on the secondary structure is available from CD spectra.^{8,9} CD measurements suggest that the peptide has a random coil structure (65–56%) in deionized water at pH 5 and 7, and an α -helical structure (58%) in TFE. A combination of random coil (38%) and β -sheet (40%) was observed in phosphate buffer at pH 7, while a β -sheet conformation (58%) was observed in phosphate buffer at pH 5. Moreover, the amidation of the C terminal decreases the propensity to adopt a β -sheet in phosphate buffer at both pH 5 and 7. Simulation results suggest (Table 2) that PrP106–126 is primarily unstructured. The percentages of secondary structure observed in the simulations is, in general, lower than those observed experimentally for uncapped PrP106–126. α -Helical elements were more persistent in hydrophobic environments, such as hexane and TFE solution, than in the more polar environments, water, and DMSO. In polar solvents, the percentage of helical structure

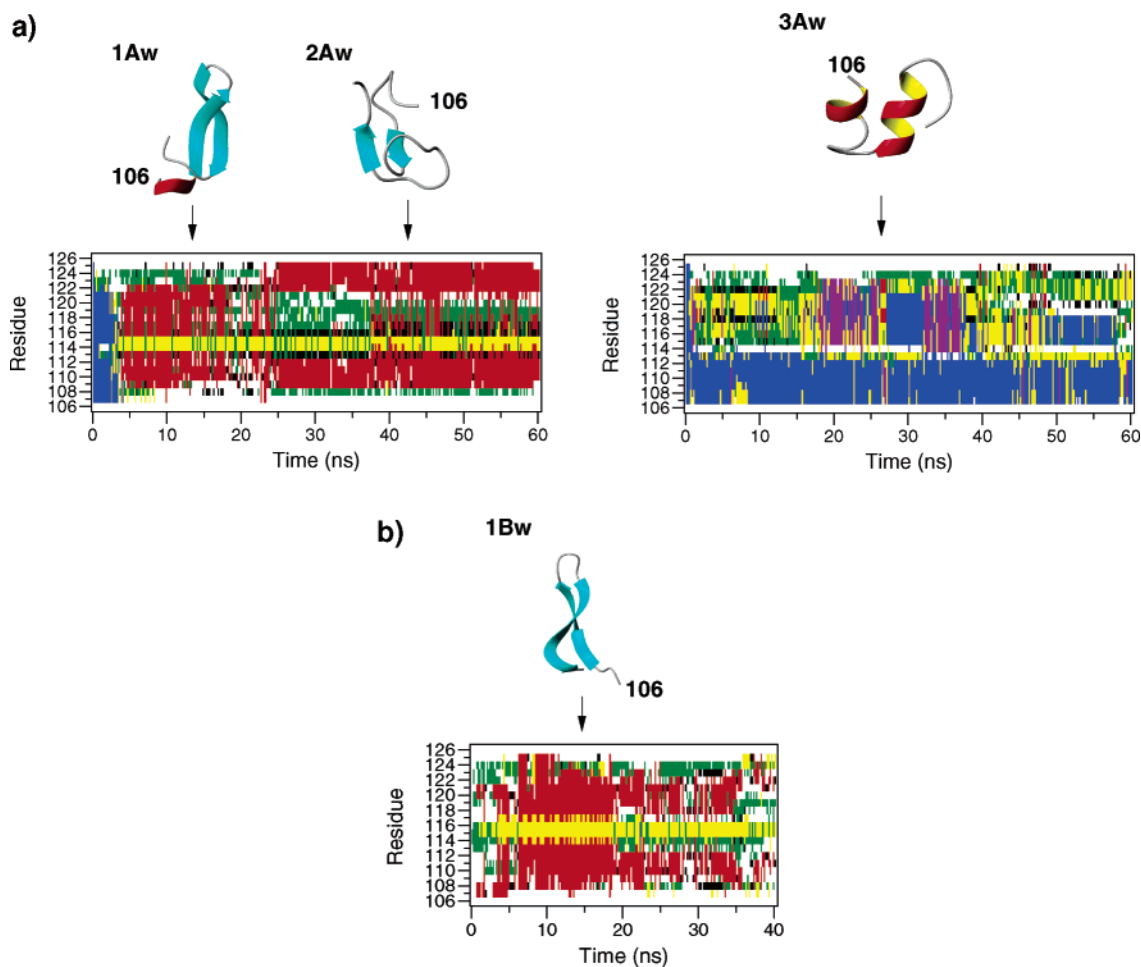


Figure 2. Secondary structure elements of PrP106–126 as a function of time for the HIS simulations in aqueous solution starting from: (a) α -helix (60 ns, 60 ns); (b) β -hairpin (40 ns). Structures: coil in white, β -sheet in red, α -helix in blue, bend in green, turn in yellow, β -bridge in black, and π -helix in purple. On the top of the graphs, the representative structures are given together with labels. The pictures are done by using the graphical program MOLMOL.³⁰

TABLE 2: Percentage of Secondary Structure in PrP106–126 Observed in the MD Simulations^a

PrP106–126 environment	% secondary structure		
	α -helix	β -sheet	random coil
water (HIS)	11	18	71
water (HISH)	7	7	86
DMSO (HIS)	1	0	99
hexane (HIS)	14	4	82
TFE (HIS)	28	2	70

^a The values are calculated omitting the first 5 ns of each simulation.

is low, between 7 and 11% in aqueous solution and 1% in DMSO. The percentages in the simulations are comparable to that inferred from CD spectra of the uncapped PrP106–126 (13% in deionized water and 15–21% in buffer solution). The highest percentage of β -sheet in the simulations (18%) was observed in water under neutral conditions, while highest percentage of β -sheet determined by CD (58%) was found at pH 5 in phosphate buffer. In the simulations in hexane, almost no β -sheet was observed. This contrasts with the 64% of β -sheet observed by CD spectra in liposomes. Note that the simulations in hexane can resemble only the hydrophobic core of the membrane. However, it should be noted that, in general, the direct comparison of simulations with the CD spectra is difficult, as relating intensities to percentage of secondary structure is context dependent. Moreover, the parameters used to relate signal intensity to structure have been fitted to proteins and may

not be fully applicable to short peptides.^{31,32} We also note that CD yields better predictions of α -helix than of β -sheet.³²

Data on the conformational behavior of PrP106–126 in solution is also available from ¹H NMR.¹⁰ In particular, spectra obtained in water at pH 3.5 and in DMSO have enough resolution to allow the measurement of proton–proton ³J coupling constants between the amide and C^α protons. The experiments were performed on the native as opposed to the amidated form of the peptide. The ³J coupling constants were also estimated from each of the simulation sets. Figure 3 shows the experimental and calculated values of ³J_{H_NH_α for PrP106–126 in water and DMSO. The experimental values at pH 3.5 have been compared with those obtained by the simulations carried out with His111 doubly protonated.}

Except for the region around residues 113–119, the agreement with the experimental data is reasonable in water (Figure 3a). Experimentally, ³J-coupling values in the 113–119 region are low (less than 6.0 Hz), indicating an α -helical conformation. In the simulations, α -helical elements were mainly observed in the hydrophilic regions. It is interesting to note that the *J*-coupling constants calculated for residues 118–126 in water showed similar values despite whether His111 was singly (HIS) or doubly (HISH) protonated (data not shown). This suggests that the protonation state of His111 does not affect the conformational behavior of the hydrophobic tail significantly.

The calculated *J*-coupling constants of PrP106–126 in DMSO show a better agreement with the experiment than the values

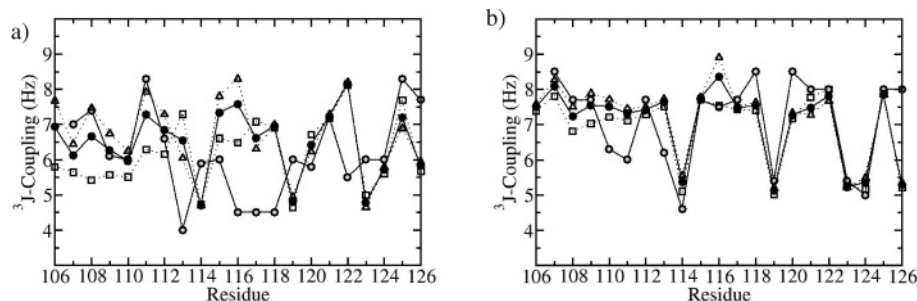


Figure 3. Values of $^3J_{\text{NH}\alpha}$ coupling constant (Hz) of PrP106–126 vs the amino acid number: (a) in water solution at pH 3.5; (b) in DMSO solution. The experimental values¹⁰ are in gray-filled circle; the computed values are in black-filled circle (A and B sets together), in open square (A set), and in open triangle (B set). The first 5 ns of each simulation were omitted when calculating the J -coupling constants.

in water (Figure 3b). Unlike in water, where many $^3J_{\text{NH}\alpha}$ values are lower than 6 Hz in water, in DMSO, most are greater than 7 Hz, suggesting that the peptide is mainly in an extended conformation.¹⁰ The secondary structure analysis of the peptide in DMSO does not show persistent secondary structure elements. The number of intramolecular H-bonds is low. On average, PrP106–126 has 1.5 intramolecular H-bonds in DMSO, while there are 7.5 in water, 8.2 in hexane, and 8.8 in TFE. The SAS of the peptide in DMSO is on average 24.7 nm², while the exposed surface to water or hexane is around 16.5–17.1 nm². The relative numbers of inter- and intramolecular H-bonds and high values of SAS reflect an elongated conformation. In all simulations in DMSO starting from an α -helix, the original structure was lost within 5 ns. This is slightly longer than in water (2 ns). This could be related to several factors. For one, the shear viscosity of the DMSO model is $1.22 \cdot 10^{-3} \text{ kg m}^{-1} \text{ s}^{-1}$,¹⁹ while for SPC, water is $0.4 \cdot 10^{-3} \text{ kg m}^{-1} \text{ s}^{-1}$.³³ The displacement of the solvent could be seen as an important determinant of the kinetics of the loss of the starting conformation.³⁴ An alternative explanation might be that water is better able to disrupt internal H-bonds.

In DMSO, there were only very small differences in the J -coupling constants between the A and B sets (Figure 3b), suggesting the simulation had converged. This was not the case in either hexane or TFE. Many J -coupling constants calculated from the simulations in hexane and TFE were below 6 Hz when the A set was analyzed (reflecting the present of the helical element) and above 7 Hz when the B set was considered. In hexane (14% α -helix), the persistent helical structures involved the hydrophilic part (residues 108–112) and the hydrophobic one (residues 114–122); in TFE (28% α -helix), the starting α -helix model never lost the initial conformation. The large differences in the J -coupling constants between the two sets in hexane and in TFE reflects the fact that 60 ns of simulation is not enough to achieve equilibrium.

Finally, it should be noted that the simulations have been performed by using a capped form of the peptide. In contrast, the experiment data is primarily available for the native form of the peptide. Experiments performed on the C-terminus amidated peptide⁹ and recent experiments on PrP[Ac-106–126-NH₂]³⁵ show that the removal of the C-terminus charge affects the conformational properties of the peptides. In water solution, the amidation of the C-terminal decreases the propensity to adopt a β -sheet, and no increase in the proportion of β -sheet was observed on varying the pH of the solution.

Conclusions

Extensive MD simulations (240 ns) have been performed to investigate the conformational behavior of isolated PrP106–126 in four different environments. The simulations suggest that

isolated PrP106–126 is mostly unstructured in solution. The peptide can adopt a metastable helical structure in more apolar solvents, such as hexane (14%) and TFE (28%). In aqueous solution, a mixture of β -sheet (18%) and helical structures (11%) were observed. In DMSO solution, the peptide is effectively random coil. The range of helical structure in the different environments is in rough agreement with that inferred from CD spectra. However, the highest probability of β -sheet formation in the simulations was observed in water, which is not supported by experiment.

In aqueous solution, a persistent element of β -sheet between residues 108–112 and either residues 115–121 or 121–126 was observed. At neutral solution, an α – β transition was observed in the simulations. When His111 was protonated, mimicking acid conditions, no α – β transitions were observed and the probability of β -sheet formation decreased, in contrast with CD data obtained at pH 5 in buffer solution. Also, the α -helical conformation in the region Ala113–Ala120 deduced by NMR experiment at pH 3.5 was not reproduced in the simulations. The extended conformation observed experimentally for PrP106–126 in DMSO solution was reproduced, with J -coupling constants from the simulations in good agreement with experiment.

In conclusion, MD simulations of PrP106–126 clearly indicate that the peptide shows conformational polymorphism in solution. Thus, they provide support to the possible role of this fragment in the structural transition of PrP^C to PrP^{Sc} in response to changes in the local environmental conditions. The results from the simulations have been verified where possible against the available experimental data. We note, however, that direct comparison is not possible, both due to the limited time scale that can be simulated and the fact that the effect of aggregation can never be fully eliminated from the experiment.

References and Notes

- (1) Prusiner, S. B. *Science* **1991**, 252, 1515.
- (2) Prusiner, S. B.; Scott, M. R.; De Armond, S. J.; Cohen, F. E. *Cell* **1998**, 93, 337.
- (3) Zhang, H.; Stockel, J.; Mehlohorn, I.; Groth, D.; Baldwin, M. A.; Prusiner, S. B.; James, T. L.; Cohen, F. E. *Biochemistry* **1997**, 36, 3543.
- (4) Pan, K. M.; Baldwin, M.; Nguyen, J.; Gasset, M.; Serban, A.; Groth, D.; Mehlohorn, I.; Huang, Z.; Fletterick, R. J.; Cohen, F. E.; Prusiner, S. B. *Proc. Natl. Acad. Sci. U.S.A.* **1993**, 90, 10962.
- (5) (a) Riek, R.; Hornemann, S.; Wider, G.; Glockshuber, R.; Wüthrich, K. *FEBS Lett.* **1997**, 413, 282. (b) Riek, R.; Hornemann, S.; Wider, G.; Billeter, M.; Glockshuber, R.; Wüthrich, K. *Nature* **1996**, 382, 180. (c) Donne, D. G.; Viles, J. H.; Groth, D.; Mehlohorn, I.; James, T. L.; Cohen, F. E.; Prusiner, S. B.; Wright, P. E.; Dyson, H. J. *Proc. Natl. Acad. Sci. U.S.A.* **1997**, 94, 13452. (d) James, T. L.; Liu, H.; Ulyanov, N. B.; Farr-Jones, S.; Zhang, H.; Donne, D. G.; Kaneko, K.; Groth, D.; Mehlohorn, I.; Prusiner, S. B.; Cohen, F. E. *Proc. Natl. Acad. Sci. U.S.A.* **1997**, 94, 10086. (e) Zahn, R.; Liu, A.; Lührs, T.; Riek, R.; von Schroetter, C.; Garcia, L.; Billeter, M.; Calzolari, L.; Wider, G.; Wüthrich, K. *Proc. Natl. Acad. Sci.*

- U.S.A. **2000**, 97, 145. (f) Knaus, K. J.; Morillas, M.; Swietnicki, W.; Malone, M.; Surewicz, W. K.; Yee, V. C. *Nat. Struct. Biol.* **2001**, 8, 770.
- (6) (a) Forloni, G.; Angeretti, N.; Chiesa, R.; Monzani, E.; Salmona, M.; Bugiani, O.; Tagliavini, F. *Nature* **1993**, 362, 543. (b) Brown, D. R.; Schmidt, B.; Kretschmer, H. A. *Nature* **1996**, 380, 345. (c) Forloni, G.; Del Bo, R.; Angeretti, N.; Chiesa, R.; Smiroldo, S.; Doni, R.; Ghibaudi, E.; Salmona, M.; Porro, M.; Verga, L.; Giaccone, G.; Bugiani, O.; Tagliavini, F. *Eur. J. Neurosci.* **1994**, 6, 1415.
- (7) (a) Tagliavini, F.; Prelli, F.; Verga, L.; Giaccone, G.; Sarma, R.; Gorevic, P.; Ghetti, B.; Passerini, F.; Ghibaudi, E.; Forloni, G.; Salmona, M.; Bugiani, O.; Frangioni, B. *Proc. Natl. Acad. Sci. U.S.A.* **1993**, 90, 9678. (b) Tagliavini, F.; Prelli, F.; Porro, M.; Rossi, G.; Giaccone, G.; Farlow, M. R.; Dlouhy, S. R.; Ghetti, B.; Bugiani, O.; Frangione, B. *Cell* **1994**, 79, 695. (c) Selvaggini, C.; De Gioia, L.; Cantù, L.; Ghibaudi, E.; Diomedede, L.; Passerini, F.; Forloni, G.; Bugiani, O.; Tagliavini, F.; Salmona, M. *Biochem. Biophys. Res. Commun.* **1993**, 194, 1380.
- (8) De Gioia, L.; Selvaggini, C.; Ghibaudi, E.; Diomedede, L.; Bugiani, O.; Forloni, G.; Tagliavini, F.; Salmona, M. *J. Biol. Chem.* **1994**, 269, 7859.
- (9) Salmona, M.; Malesani, P.; De Gioia, L.; Gorla, S.; Bruschi, M.; Molinari, A.; Della Vedova, R.; Pedrotti, B.; Marrari, M. A.; Awan, T.; Bugiani, O.; Forloni, G.; Tagliavini, F. *Biochem. J.* **1999**, 342, 207.
- (10) Ragg, E.; Tagliavini, F.; Malesani, P.; Monticelli, L.; Bugiani, O.; Forloni, G.; Salmona, M. *Eur. J. Biochem.* **1999**, 266, 1192.
- (11) Kuwata, K.; Matumoto, T.; Cheng, H.; Nagayama, K.; James, T. L.; Roder, H. *Proc. Natl. Acad. Sci. U.S.A.* **2003**, 100, 14790.
- (12) Terzi, E.; Hölzemann, G.; Seelig, J. *Biochemistry* **1994**, 33, 1345.
- (13) Levy, Y.; Hanan, E.; Solomon, B.; Becker, O. M. *Proteins* **2001**, 45, 382.
- (14) (a) Kazmirski, S. L.; Alonso, D. O. V.; Cohen, F. E.; Prusiner, S.B.; Daggett, V. *Chem. Biol.* **1995**, 2, 305. (b) Daidone, I.; Simona, F.; Roccatano, D.; Broglia, R. A.; Tiana, G.; Colombo, G.; Di Nola, A. *Proteins* **2004**, 57, 198.
- (15) Inouye, H.; Kirschner, D. A. *J. Struct. Biol.* **1998**, 122, 247.
- (16) *MAESTRO Molecular Modeling Interface*, version 4.1.012; Schrödinger Inc.: Portland, OR, 2003.
- (17) (a) van Gunsteren, W. F.; Billeter, S. R.; Eising, A. A.; Hünenberger, P. H.; Krüger, P.; Mark, A. E.; Scott, W. R. P.; Tironi, I. G. *Biomolecular Simulation: The GROMOS96 Manual and User Guide*; Vdf Hochschulverlag AG an der ETH Zürich: Zürich, 1996. (b) Schuler, L. D.; van Gunsteren, W. F. *Mol. Sim.* **2000**, 25, 301.
- (18) Berendsen, H. J. C.; Postma, J. P. M.; van Gunsteren, W. F.; Hermans, J. In *Intermolecular Forces*; Pulman, B., Ed.; D. Reidel Publishing Company: Dordrecht, The Netherlands, 1981; p. 331.
- (19) Geerke, D. P.; Oostenbrink, C.; van der Vegt, N. F. A.; van Gunsteren, W. F. *J. Phys. Chem. B* **2004**, 108, 1436.
- (20) Fioroni, M.; Burger, K.; Mark, A. E.; Roccatano, D. *J. Phys. Chem. B* **2000**, 104, 12347.
- (21) (a) Berendsen, H. J. C.; van der Spoel, D.; van Drunen, R. *Comput. Phys. Commun.* **1995**, 91, 43. (b) Lindahl, E.; Hess, B.; van der Spoel, D. *J. Mol. Model.* **2001**, 7, 306.
- (22) Tironi, I. G.; Sperb, R.; Smith, P. E.; van Gunsteren, W. F. *J. Chem. Phys.* **1995**, 102, 5451.
- (23) Berendsen, H. J. C.; Postma, J. P. M.; van Gunsteren, W. F.; Di Nola, A.; Haak, J. R. *J. Chem. Phys.* **1984**, 81, 3684.
- (24) Miyamoto, S.; Kollman, P. A. *J. Comput. Chem.* **1992**, 13, 952.
- (25) Hess, B.; Bekker, H.; Berendsen, H. J. C.; Fraaije, J. G. E. M. *J. Comput. Chem.* **1997**, 18, 1463.
- (26) Eisenhaber, F.; Lijnzaad, P.; Argos, P.; Sander, C.; Scharf, M. *J. Comput. Chem.* **1995**, 16, 273.
- (27) Kabsch, W.; Sander, C. *Biopolymers* **1983**, 22, 2577.
- (28) Karplus, M. *J. Chem. Phys.* **1959**, 30, 11.
- (29) Vuister, G. W.; Bax, A. *J. Am. Chem. Soc.* **1993**, 115, 7772.
- (30) Koradi, R.; Billeter, M.; Wüthrich, K. *J. Mol. Graphics* **1996**, 14, 51.
- (31) Yang, J. T.; Wu, C. C.; Martinez, H. M. *Methods Enzymol.* **1986**, 130, 208.
- (32) Johnson W. C., Jr. *Annu. Rev. Biophys. Biophys. Chem.* **1988**, 17, 145.
- (33) Hess, B. *J. Chem. Phys.* **2002**, 116, 209.
- (34) Sacob, M.; Schmid, F. X. *Biochemistry* **1999**, 38, 13773.
- (35) Di Natale, G.; Impellizzeri, G.; Pappalardo, G.; *Org. Biomol. Chem.* **2005**, 3, 490.